Supporting Material for

Relating Introspective Accuracy to Individual Differences in Brain Structure

Stephen M. Fleming,* Rimona S. Weil, Zoltan Nagy, Raymond J. Dolan, Geraint Rees

*To whom correspondence should be addressed. E-mail: s.fleming@fil.ion.ucl.ac.uk

Materials and Methods

Participants

32 participants (15 males; aged 19 – 37 years; mean age 26.4 years) gave written informed consent to take part in the experiment. The study was approved by the local Research Ethics Committee. One participant was excluded from further analysis of brain structure due to aberrant psychophysical task performance (*d'* > 3SD from the group mean).

Stimuli

The perceptual decision display comprised six Gabor gratings (circular patches of smoothly varying light and dark bars) arranged around a central fixation point (Fig 1). Each Gabor subtended 1.4 degrees of visual angle in diameter, and consisted of a luminance pattern modulated at a spatial frequency of 2.2 cycles per degree. Each "baseline" Gabor had a contrast of 20% of maximum, and appeared at a mean eccentricity of 6.9 degrees. The fixation point comprised a black square measuring 0.2 degrees across, luminance 0.10 cd/m^2, with a central white square 0.1 degrees across, luminance 13.64 cd/m^2. The background was a uniform gray screen of luminance 3.66 cd/m^2.

Baseline Gabors were displayed with a contrast of 20% (where 0% is no difference between the luminance of the grating bars and 100% is maximum difference, i.e. black to white). The pop-out Gabors were drawn from a stimulus set in which contrast varied from 23 to 80% in increments of 3%. At the time of confidence ratings, the display consisted of a grey screen (luminance 3.66 cd/m^2) with the numbers 1 to 6 written left to right (luminance 13.64 cd/m^2, 0.7 degrees in height, centred around fixation).

Stimuli were presented on a gamma calibrated CRT display (Dell FP2001, 20.1 inch display; 800 x 600 pixels; 60 Hz refresh rate), at a viewing distance of approximately 60 cm, situated in a darkened room. Stimulus display and response collection were controlled by Matlab 7.8.0 (Mathworks Inc., Natick, MA, USA) using the COGENT 2000 toolbox (http://www.vislab.ucl.ac.uk/cogent.php).

Task

The visual judgement comprised a temporal two-alternative forced choice pop-out task (see Fig. 1 for timings). All the Gabors in one interval were of the same contrast, but in the other interval, one of the Gabors was of a higher contrast than the others (the "pop-out" Gabor, illustrated by a dashed circle in Fig. 1 that was not present in the actual display). The temporal interval and spatial position of the pop-out Gabor varied randomly between trials. Participants were required to decide whether this pop-out Gabor had appeared in the first or the second interval. The perceptual judgement was indicated by participants using the left hand with the numbers '1' (first interval) or '2' (second interval) on the QWERTY keypad of a standard PC keyboard. Participants then indicated their confidence in the perceptual decision they had just made on a scale of 1 (low relative confidence) to 6 (high relative confidence), using their right hand to press

one of the numbers '1' to '6' on the numerical keypad. A square red frame (width 1 degree, thickness 0.1 degree) appeared around the selected rating (Fig. 1).

The contrast of the pop-out Gabor was chosen from the stimulus set of pop-out Gabors using a 1-up 2-down staircase procedure (*S1*), which at the limit results in convergence on 71% accuracy. The contrast of the pop-out Gabor at the end of each block was used as the starting contrast for the pop-out Gabor in the next block. Our aim in this staircase procedure was to equate objective perceptual performance across individuals, leaving quantification of metacognitive ability unconfounded by performance (*S2*).

Participants were instructed to try to use the whole of the confidence scale in their responses, and to bear in mind that the scale represents relative confidence, as, given the difficult nature of the task, they would rarely be completely certain that their visual judgement had been correct. Participants performed a practice session to familiarise themselves with the stimuli and task. The main experiment consisted of 600 trials, split into 6 blocks of 100 trials. They were given no feedback about their performance until the end of the experiment.

Quantification of metacognitive ability

The accuracy of metacognitive assessments can be intuited as how transparent an initial perceptual decision process is to a putative "higher" level assessment. This intuition can be captured within the logic of signal detection theory (SDT), which assesses how faithfully a creature separates signal from noise. Conventional applications of SDT assess detection performance by comparing the proportion of "hits" and "false alarms" in a stimulus detection task. By applying the logic of SDT to metacognition ("Type 2" SDT), we categorised a "hit" as a high confidence response after a correct decision and a "false alarm" as a high confidence response after an incorrect decision [see table S1 and (*S3*)]. Because the specific mathematical assumptions of conventional SDT may not hold for this new analysis (*S4*, *S5*), we used nonparametric assessments of sensitivity and bias (*S6*). We constructed Type 2 ROC curves for each participant (Fig. 2A and fig. S2) that characterised the probability of being correct for a given level of confidence. ROC curves were anchored at [0, 0] and [1, 1]. An ROC curve that bows sharply upwards indicates that the probability of being correct rises rapidly with confidence; conversely, a flat ROC function indicates a weak link between confidence and accuracy.

We noted a practice effect in the staircase parameters (fig. S1) reflected in a decrease in mean contrast and variability from block 1 to 2. A one-way ANOVA of mean contrast with block as a within-subjects factor revealed a significant effect of block ($F_{(5,155)} = 8.18$, $P < 0.001$) that was abolished on removal of block 1 ($F_{(4,124)} = 1.56$, $P = 0.19$). ROC analysis was therefore carried out on data from blocks 2-6, after stabilisation of psychophysical performance. To plot the ROC, $h_i = p(\text{confidence} = i \mid \text{correct})$ and $f_i = p(\text{confidence} = i \mid \text{incorrect})$ were calculated for all i. These probabilities were then transformed into cumulative probabilities, and plotted against each other (Fig. 2A and fig. S2). Following Kornbrot (*S6*), we computed distribution-free measures of sensitivity and bias from this ROC by dividing the area into two parts – K_B is the area between the ROC curve and the major diagonal (solid line in Fig. 2A) to the right of the minor diagonal (dotted line in Fig. 2A), and K_A is the area between the

ROC curve and major diagonal to the left of the minor diagonal. From simple geometry [derived in the Appendix of (*S6*)], these areas can be calculated as follows:

$$K_A = \frac{1}{4}\sum_{k=1}^{k=\frac{1}{2}i}[(h_{k+1} - f_k)^2 - (h_k - f_{k+1})^2]$$

$$K_B = \frac{1}{4}\sum_{k=\frac{1}{2}i}^{k=i}[(h_{k+1} - f_k)^2 - (h_k - f_{k+1})^2]$$

Sensitivity (A_{roc}) is then the sum of these areas, and Type 2 bias (B_{roc}) is the log of the ratio:

$$A_{roc} = K_A + K_B$$

$$B_{roc} = \ln(\frac{K_A}{K_B})$$

Type I *d'* and bias (*c*) were calculated in the standard manner (*S7*):

$d' = 1/\sqrt{2}\ [z(H) - z(F)]$

$c = -0.5\ [z(H) + z(F)]$

where *z* is the inverse of the cumulative normal distribution function, $H = p(\text{response} = 1|\text{interval} = 1)$ and $F = p(\text{response} = 1|\text{interval} = 2)$. Confirmatory correlation analyses between SDT parameters and grey matter (GM)/fractional anisotropy (FA) clusters [signal extracted using the MarsBar toolbox (*S8*)] were carried out using Pearson's product-moment correlations in SPSS 17.0.

Voxel-based morphometry analysis

Voxel-based morphometry (VBM) provides a quantitative measure (at each voxel) of the tissue volume per unit volume of spatially normalised image (*S9*). A 1.5T Sonata scanner (Siemens Medical Systems, Erlangen, Germany) was used to acquire all images for each participant. T1-weighted anatomical whole-brain scans were acquired for VBM analysis (176 slices, echo time = 3.56ms, TR = 12.24ms, voxel size 1mm isotropic). VBM preprocessing was carried out using SPM8 (http://www.fil.ion.ucl.ac.uk/spm). The images were first segmented into GM, white matter (WM) and cerebral spinal fluid in native space (*S10*). The GM segment images from this process were then rigidly aligned and subsequently warped to an iteratively improved template using nonlinear registration in DARTEL (*S11*). DARTEL's "Normalise to MNI" module was then used to produce smoothed normalised images. The DARTEL template was affinely registered to MNI space, and the GM images were transformed using the DARTEL flow-fields and this affine transformation, in a way that preserved their local tissue

volumes (equivalent to a Jacobian "modulation" step). Smoothing used a Gaussian kernel of 8mm full width at half maximum.

The pre-processed GM images were entered into a multiple regression model in SPM8 to determine which brain regions showed significant covariation with the SDT-based measures of metacognitive ability. We included A_{roc}, *d'*, Type II criterion (B_{roc}; the overall tendency to use high confidence responses), the absolute (unsigned) value of the Type I criterion (|*c*|) and gender (M = 1; F = 0) in the model. Type I criterion (*c*) measures the extent of the bias towards interval 1 or 2 on the perceptual decision task, with greater bias reflecting suboptimal performance. Positive values indicate bias towards interval 1, and negative values bias towards interval 2. We thus entered the absolute value of *c* as a covariate of no interest, with higher values indicating suboptimal performance bias towards either interval.

Adjustment for "global" brain volume using proportional scaling was applied, resulting in voxel values that were proportions of total GM volume. A binary mask (SPM8 grey.nii template > 0.3) was used to restrict the search volume to changes in GM. T-statistic maps reflecting the correlation between each regressor and regional GM volume were created. Cluster-based statistics were used to locate significant regions based on both their peak value and spatial extent after applying an initial cluster-defining threshold of $P < 0.001$. Due to structural images displaying local variation in smoothness, standard applications of cluster-based random field theory are inappropriate (*S12*). We thus applied non-stationary cluster extent correction when calculating family-wise error (FWE) corrected *P* values using the NS toolbox (http://www.fmri.wfubmc.edu/cms/NS-General). Computational simulations (*S12*) show that for designs with high degrees of freedom and sufficient smoothness, as here, using a cluster defining threshold of $P < 0.001$ with correction for non-stationarity provides adequate control over the family-wise false positive rate ($P < 0.05$).

Diffusion tensor imaging analysis

The diffusion tensor imaging (DTI) dataset comprised of 68 images with 60 slices and 2.3 mm isotropic resolution. The first 7 images were collected with b = 100 s/mm^2. The diffusion encoding directions were isotropically distributed on the surface of the sphere (*S13*) for the remaining 61 images and the b-value was 1000 s/mm^2. The echo time was 90ms, each 2D image slice took 150ms to collect, and the field of view was 220mm. DTI data sets are often collected using echo-planar imaging (EPI) methods which are affected by susceptibility-induced artefacts. To reduce the extent of these artefacts two datasets were collected for each participant, with the only difference being that the phase encoding direction was reversed for the second run. This method ensures the susceptibility-induced distortions are equal and opposite in the two datasets, providing the opportunity to correct their effect (*S14*).

Diffusion-weighted images were first aligned using FSL's eddycorrect **(**http://www.fmrib.ox.ac.uk/fsl/**)**, and then combined into a single dataset with reduced susceptibility-induced artefacts. The main diffusion tensor was then fitted at each voxel using FSL's dtifit. From the tensor a rotationally invariant measure of diffusion anisotropy can be calculated. One such measure is fractional anisotropy (FA) with values ranging from 0 (representing isotropic, or undirected, diffusion) to 1

(representing a single preferred direction of diffusion). This measure has been used extensively to investigate local WM integrity, as diffusion of water molecules is more restricted perpendicular to, rather than along, neuronal fibres. The calculated FA map for each participant (in native space) was imported into SPM8 and coregistered to the WM segment image of the same participant created during VBM analysis. Coregistration was carried out by maximising normalised mutual information between the images. The DARTEL flowfields and affine (MNI) transformation were then applied to each participant's coregistered FA image, producing normalised FA images in MNI space. Unlike the VBM normalisation (which preserved the original local tissue volume), the FA images were normalised in a way that preserved their original voxel values (without "modulation"). Normalised FA images were also smoothed with a 8mm full-width at half maximum Gaussian kernel prior to statistical analysis. For one participant, DTI scans were unavailable, leaving 30 subjects in the FA analysis.

Statistical analysis of FA proceeded in an identical fashion to that of GM volume (see above). A multiple regression model was constructed consisting of A_{roc}, *d'*, Type II criterion (B_{roc}; the overall tendency to use high confidence responses) and the absolute (unsigned) value of the Type I criterion ($|c|$). A binary mask (mean normalised FA > 0.2) was used to restrict the search volume to changes in WM. Statistical inference was conducted as for VBM. Probable tract labels were obtained using the JHU White-Matter Tractography Atlas within FSL.

ROC model fits

To explore how well a Gaussian Type II SDT model accounted for the confidence rating data (*S7*), we fit the following linear regression model:

$$z(h) = \beta_0 + \beta_1 z(f) + \varepsilon$$

where z is the inverse of the cumulative normal distribution function. This model provided an excellent fit to the data (mean $R^2 = 0.97$), indicating that the underlying $f(X|\text{correct})$ and $f(X|\text{incorrect})$ distributions are normal-like [where X is a random decision variable; see (*S4*) for further details]. The β_1 parameter (slope) indicates the relative variance of the two distributions. This parameter was on average less than 1 within our sample (0.88 ± 0.026 SEM), indicating that the $f(X|\text{correct})$ distribution has greater variance than the $f(X|\text{incorrect})$. Interestingly, theoretical models that suggest a direct translation of Type I into Type II distributions predict a Type II ROC slope slightly less than 1 (*S4*). However, this picture is not clear-cut: recent metamemory data support an equal-variance Gaussian model (*S15*). We note that our use of nonparametric methods to characterise A_{roc} are not dependent on the specific form of the model used; indeed, it was the methodological uncertainty surrounding the quantification of Type II processes that led us to adopt the distribution-free approach (*S6*).

Control analyses of GM and FA correlations

We carried out additional analysis to rule out potential alternative interpretations of our findings. One concern is that variation in underlying perceptual acuity could confound the anatomical variance we ascribe to metacognitive ability (A_{roc}). Good perceptual ability may be reflected in low mean stimulus contrast and/or low staircase variability

(though we note that extraneous environmental or ocular factors also affect these variables). To rule out this interpretation, we computed the partial correlation between brain structure and A_{roc} while controlling for both mean stimulus contrast and the variability (SD) in the staircase required to achieve a constant level of performance within each individual. Both the GM cluster in BA10 ($r = 0.39$, $P = 0.036$) and the FA cluster in anterior corpus callosum ($r = 0.74$, $P < 0.001$) remained significantly correlated with A_{roc} after controlling for mean contrast and staircase variability.

This partial correlation analysis only examines the correlation of predefined regions. As a further test, we constructed a second design matrix in which mean stimulus contrast and staircase variability were directly entered as predictors of GM/FA, with gender again present as a covariate of no interest. Neither measure correlated with grey matter or FA at the statistical thresholds used in the main analysis ($P > 0.05$, corrected for multiple comparisons), even when applying a mask (8mm sphere) to isolate voxels within the vicinity of the BA10 (GM) or the anterior corpus callosum (FA) peak voxels. While we are cautious in interpreting uncorrected findings, one result of potential interest is that GM volume in the medial calcarine sulcus, consistent with the location of early visual cortex, showed increased volume in subjects with greater perceptual acuity as defined by negative mean stimulus contrast ($P < 0.001$, uncorrected). Table S4 details uncorrected results from these models for completeness. Together these control analyses indicate that the correlations we observe between A_{roc} and structure relate to differences in metacognitive ability rather than low-level differences in performance.

Negative correlations with A_{roc}

We found negative correlations with A_{roc} in bilateral regions of anterior inferior temporal grey matter (left, $P < 0.05$, corrected for multiple comparisons; right, $P < 0.001$, uncorrected; table S3). While we are cautious about interpreting the relevance of a decrease in grey matter volume for increased metacognitive ability, we note that these temporopolar regions have been implicated in both self-related (*S16*) and higher-order visual (*S17*) processing, and thus alterations in grey matter here might similarly place functional constraints on perceptual metacognition.

Figure S1

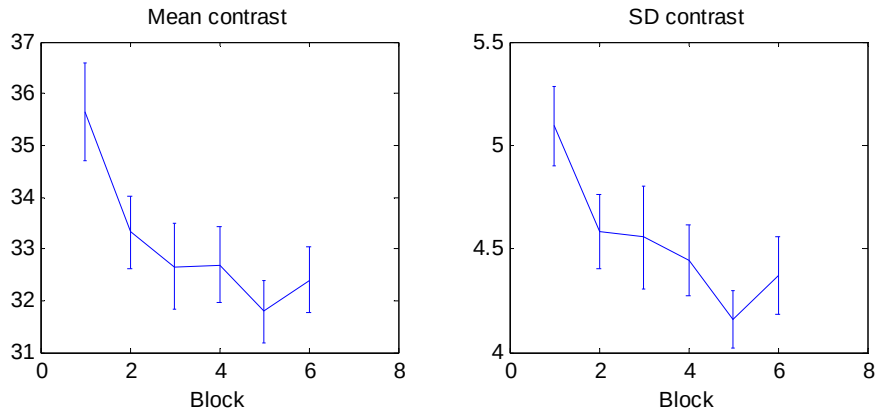

Stimulus parameters for the behavioural task. Mean and standard deviation (SD) of oddball Gabor contrast (percentage of maximum contrast) plotted for each block of the perceptual task, averaged over participants. Error bars represent one standard error of the mean. Because stimulus contrast and variability were significantly higher in Block 1 (see Methods), indicating a period of gradual stabilisation of performance, only data from blocks 2-6 were used to calculate SDT measures.

Figure S2

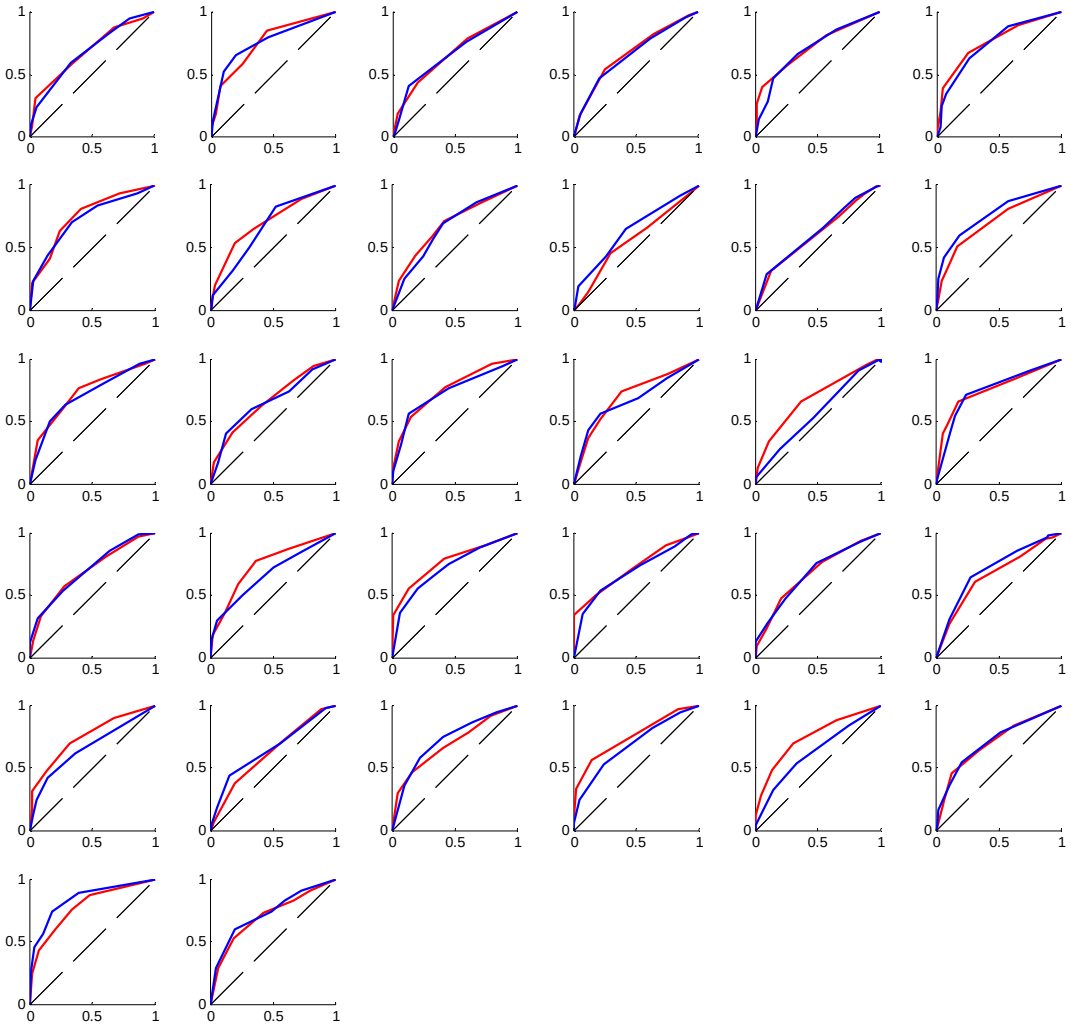

Individual ROC curves calculated from the behavioural data (see Materials and Methods & Fig. 2) plotted for each of the 32 participants, split into odd (blue; blocks 3 and 5) and even (red; blocks 2, 4 and 6) blocks of the psychophysics session.

Figure S3

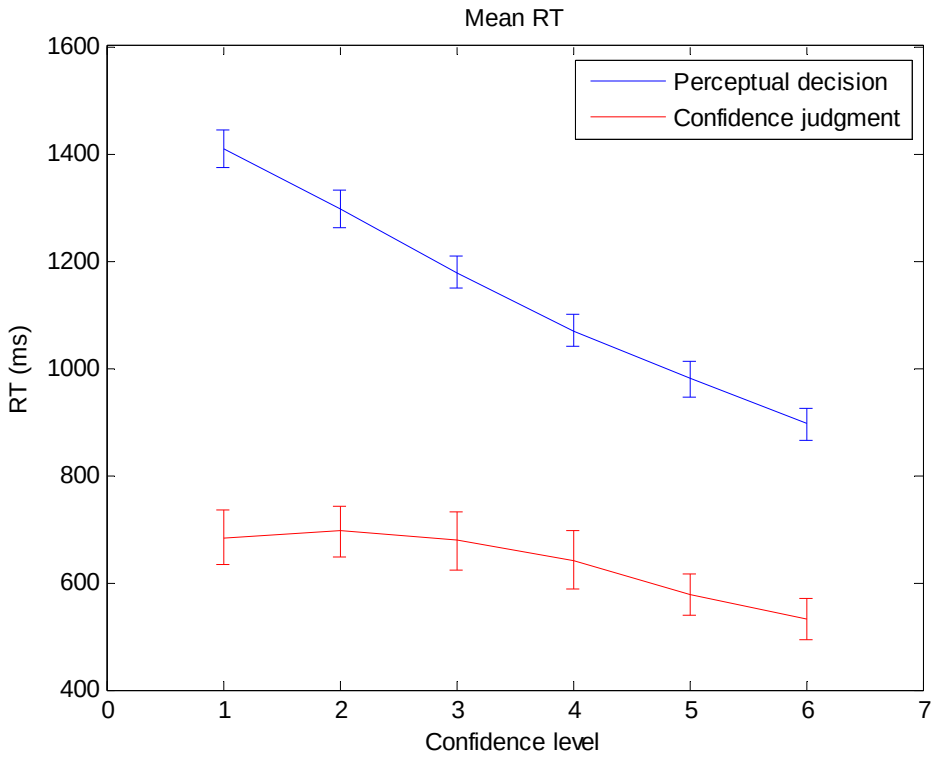

Mean reaction times (RT) measured in milliseconds for both the perceptual decision (blue) and the confidence judgment (red) from blocks 2-6, plotted as a function of reported confidence level. Data are averaged across 32 participants and the error bars represent one standard error of the mean.

Figure S4

(A)

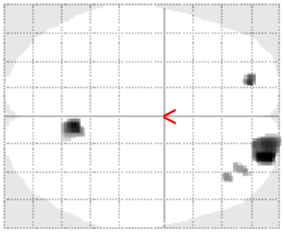

(B)

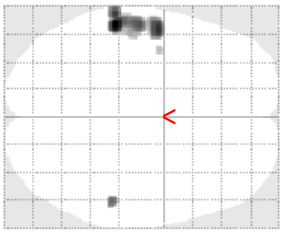

(C)

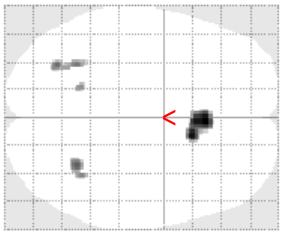

Axial "glass brains" (viewed from above) showing areas where grey matter volume correlates positively (**A**) and negatively (**B**) with A_{roc}, and where white matter fractional anisotropy correlates positively with A_{roc} (**C**). No suprathreshold fractional anisotropy clusters were found for negative correlations with A_{roc} (see also tables S2 and S3). All maps are thresholded at $P < 0.001$, uncorrected with an extent threshold of 10 voxels.

Table S1

Classification of responses within Type II signal detection theory, assuming binary confidence ratings. In our task, we used graded confidence ratings, allowing computation of Type II sensitivity from the full ROC function.

Type I decision	**High confidence**	**Low confidence**
Correct	Hit	Miss
Incorrect	False alarm	Correct rejection

Table S2

GM volume associated with behavioural variables (SDT parameters) entered into the multiple regression model. Whole-brain corrected clusters ($P < 0.05$, corrected for multiple comparisons) are indicated in bold type. For completeness, correlations that survive a height threshold of $P < 0.001$, uncorrected, and an extent threshold of 10 voxels are also reported. Abbreviations: PFC – prefrontal cortex; BA – Brodmann area.

Regressor	Number of voxels	Peak voxel Z-score	*P* value (cluster FWE corrected)	Peak voxel MNI coordinates	Laterality	Label
A_{roc}	**675**	**4.02**	**0.029**	**24 65 18**	**R**	**Anterior PFC (BA10)**
	291	3.93	0.191	6 -57 18	L/R	Precuneus/posterior cingulate
	31	3.78	0.703	-20 53 12	L	Anterior PFC (BA10)
	25	3.45	0.829	36 39 21	R	Dorsolateral PFC (BA46)
	29	3.44	0.497	33 50 9	R	Anterior PFC (BA10)
Negative A_{roc}	**713**	**3.92**	**0.026**	**-56 -30 -26**	**L**	**Inferior temporal gyrus**
	76	3.69	0.753	-63 -30 10	L	Superior Temporal gyrus
	80	3.54	0.457	51 -33 -21	R	Inferior temporal gyrus
	15	3.22	0.995	-41 -3 -48	L	Inferior temporal gyrus
B_{roc}	28	3.93	0.313	-33 -73 34	L	Occipital lobe (BA19)
Negative B_{roc}	93	3.47	0.233	-59 -27 -14	L	Middle temporal gyrus
	20	3.35	0.826	-66 -10 3	L	Superior temporal gyrus
d'	82	3.77	0.175	-3 -84 -21	L/R	Cerebellum
	16	3.68	0.939	53 -25 -15	R	Middle temporal sulcus
	389	3.66	0.112	60 -39 51	R	Superior parietal
	47	3.45	0.817	6 -61 4	L/R	Lingual gyrus
	18	3.26	0.953	-3 -9 66	L	Supplementary motor area (BA6)
Negative d'	N/A	N/A	N/A	N/A	N/A	No suprathreshold clusters

Table S3

White matter microstructure (fractional anisotropy; FA) associated with behavioural variables (SDT measures) entered into the multiple regression model. Clusters that survive correction for multiple comparisons ($P < 0.05$) are indicated in bold type. For completeness, correlations that survive a height threshold of $P < 0.001$, uncorrected, and an extent threshold of 10 voxels are also reported.

Regressor	Number of voxels	Peak voxel Z-score	*P* value (cluster FWE corrected)	Peak voxel MNI coordinates	Laterality	Label
A_{roc}	**308**	**3.93**	**0.033**	**2 26 -2**	**L/R**	**Genual corpus callosum**
	66	3.58	0.492	29 -55 -2	R	Posterior corpus callosum (forceps major)
	31	3.54	0.502	-32 -67 0	L	Inferior fronto-occipital fasciculus
	26	3.48	0.680	-32 -55 14	L	Longitudinal fasciculus
	13	3.44	0.824	35 -52 -15	R	Inferior longitudinal fasciculus
	11	3.39	0.631	-18 -52 28	L	Cingulum
Negative A_{roc}	N/A	N/A	N/A	N/A	N/A	No suprathreshold clusters
B_{roc}	N/A	N/A	N/A	N/A	N/A	No suprathreshold clusters
Negative B_{roc}	128	4.24	0.226	-8 20 -9	L	Genual corpus callosum
	49	3.91	0.132	26 -51 -9	R	Posterior corona radiata
	21	3.54	0.438	-18 29 24	L	Cingulum
d'	74	3.89	0.251	-17 6 39	L	Superior corona radiata
	18	3.33	0.721	-18 -7 45	L	Superior corona radiata
Negative *d'*	N/A	N/A	N/A	N/A	N/A	No suprathreshold clusters

Table S4

GM correlating with negative stimulus contrast and staircase variability (low-level measures of perceptual performance). After correcting for multiple comparisons, no significant clusters were observed, but correlations that survive a height threshold $P < 0.001$, uncorrected, and an extent threshold of 10 voxels are reported for completeness.

Analysis	Regressor	Number of voxels	Peak voxel Z-score	*P* value (cluster FWE corrected)	Peak voxel MNI coordinates	Laterality	Label
GM	Negative mean contrast	88	3.67	0.917	14 -10 24	R	Caudate
		51	3.56	0.783	-65 -57 4	L	Middle temporal gyrus
		78	3.44	0.913	5 -76 21	L/R	Calcarine sulcus
		80	3.38	0.908	3 36 42	L/R	Dorsal medial prefrontal cortex
		11	3.21	0.982	-14 29 -20	L	Orbitofrontal cortex
	Negative SD	128	4.00	0.301	59 -42 1	R	Middle temporal gyrus
		29	3.70	0.577	-51 -33 36	L	Inferior parietal
		34	3.36	0.938	47 -15 -48	R	Postcentral gyrus
		22	3.24	0.953	-44 -21 46	L	Postcentral gyrus
FA	Negative mean contrast	N/A	N/A	N/A	N/A	N/A	No suprathreshold clusters
	Negative SD	30	3.86	0.942	-29 -15 48	L	Superior corona radiata

References

S1. H. Levitt, Transformed up-down methods in psychoacoustics. *J. Acoust. Soc. Am.* **49**, Suppl (1971).

S2. H.C. Lau, in *Frontiers of Consciousness*, Eds. L. Weiskrantz, M. Davies (Oxford University Press: 2008), pp. 245-258.

S3. C. Kunimoto, J. Miller, H. Pashler, Confidence and accuracy of near-threshold discrimination responses. *Conscious. Cogn.* **10**, 294 (2001).

S4. S.J. Galvin, J.V. Podd, V. Drga, J. Whitmore, Type 2 tasks in the theory of signal detectability: discrimination between correct and incorrect decisions. *Psychon. Bull. Rev.* **10**, 843 (2003).

S5. S. Evans, P. Azzopardi, Evaluation of a 'bias-free' measure of awareness. *Spat.Vis.* **20**, 61 (2007).

S6. D.E. Kornbrot, Signal detection theory, the approach of choice: model-based and distribution-free measures and evaluation. *Percept. Psychophys.* **68**, 393 (2006).

S7. N. Macmillan, C. Creelman, *Detection theory: a user's guide*. (Lawrence Erlbaum: New York, 2005).

S8. M. Brett, J. Anton, R. Valabregue, J. Poline, Regions of interest analysis using an SPM toolbox. *Presented at the 8th International Conference on Functional Mapping of the Human Brain* (2002).

S9. J. Ashburner, K.J. Friston, Voxel-based morphometry--the methods. *NeuroImage* **11**, 805 (2000).

S10. J. Ashburner, K.J. Friston, Unified segmentation. *NeuroImage* **26**, 839 (2005).

S11. J. Ashburner, A fast diffeomorphic image registration algorithm. *NeuroImage* **38**, 95 (2007).

S12. S. Hayasaka, K.L. Phan, I. Liberzon, K.J. Worsley, T.E. Nichols, Nonstationary cluster-size inference with random field and permutation methods. *NeuroImage* **22**, 676 (2004).

S13. K.M. Jansons, D.C. Alexander, Persistent angular structure: new insights from diffusion MRI data. *Inf. Process. Med. Imaging* **18**, 672 (2003).

S14. J.L.R. Andersson, S. Skare, J. Ashburner, How to correct susceptibility distortions in spin-echo echo-planar images: application to diffusion tensor imaging. *NeuroImage* **20**, 870 (2003).

S15. P.A. Higham, No special K! A signal detection framework for the strategic

regulation of memory accuracy. *J. Exp. Psychol. Gen.* **136**, 1 (2007).

S16. U. Frith, C.D. Frith, Development and neurophysiology of mentalizing. *Philos. T. R. Soc. B.* **358**, 459 (2003).

S17. C.G. Gross, S.D. Schonen, Representation of visual stimuli in inferior temporal cortex. *Philos. T. R. Soc. B.* **335**, 3 (1992).